Overview

The Continuum Field Approach to Modeling Microstructural Evolution

Long-Qing Chen and Yunzhi Wang

The majority of advanced engineering materials contain multiphase and/or multidomain structures. Their physical and mechanical properties depend strongly on the number of phases present and their mutual arrangement; the volume fraction of each phase; and the shape, size, and size distribution of domains (or grains). This article describes a continuum diffuse-interface field approach to modeling microstructural evolution and its application to a number of different processes, including precipitation reactions through nucleation and growth, structural transformations involving symmetry changes, and curvature-driven grain growth.

INTRODUCTION

Microstructures are thermodynamically unstable features that evolve with time. The driving force for the temporal evolution of a microstructure usually consists of one or more of the following:

- A reduction in the bulk-chemical free energy.
- A decrease of the total interfacial energy between different phases or between different orientation domains or grains of the same phase.
- Relaxation of the elastic-strain energy generated by the lattice mismatch between different phases or different orientation domains.
- External fields such as applied stress, electrical, temperature, and magnetic fields.

The phase changes and related microstructural development driven by the decrease of the bulk-chemical free energy are usually considered as phase transformations, whereas, the microstructural evolution driven by the reduction in the total interfacial free energy is called coarsening.

In the conventional treatment of interface motion, a multiphase and/or multidomain heterogeneous microstructure is characterized solely by the geometry of sharp interfacial boundaries between different phases and/or between structural domains of different orientations. These boundaries are mathematical interfaces of zero thickness. The phases and domains are assumed to have a fixed composition and structure. The dynamic evolution of a microstructure is obtained by solving a set of differential equations in each phase and/or domain with boundary conditions specified at the interfaces that are moving with time. Such a moving-boundary or free-boundary problem for complicated microstructures is impossible to solve analytically and very difficult numerically. Moreover, different processes (e.g., phase transformations, grain growth, and Ostwald ripening) have usually been treated separately using different physical models.

In order to overcome these difficulties, there has been increasing interest in the last few years in using the diffuse-interface field model to model microstructural evolution. Different from the conventional sharp-interface approach, the field model describes a heterogeneous state consisting of phases and/or domains as a whole by using a set of field variables that are functions of spatial coordinates. The most familiar example of a field variable is the composition or concentration field, which characterizes compositional heterogeneities. The temporal evolution of these field variables is then described by time-dependent kinetic field equations.

The main objective of this article is to give a brief account of the diffuse-interface field model and its applications to modeling microstructural evolution, ranging from structural transformations to grain growth in a number of different processes in solids. It should be pointed out that the references cited are just a few examples of the recent applications of the diffuse-interface field model to various processes and are, by no means, complete.

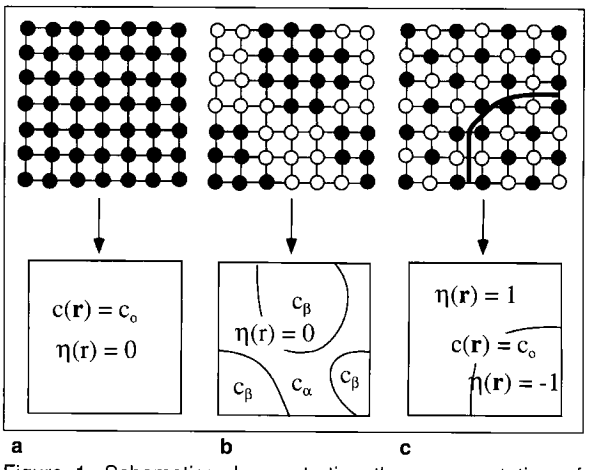

Figure 1. Schematics demonstrating the representation of morphologies by field variables. (a) disordered single phase, (b) two-phase mixture, and (c) ordered single phase.

DIFFUSE-INTERFACE FIELD MODEL

Description of Microstructures

Microstructures in the field model are described by a set of spatially dependent field variables from which the spatial distributions of grains and/or domains of different phases and the boundaries between them can be analyzed. For the purpose of demonstration, three rather simple examples are schematically shown in Figure 1: a homogeneous disordered phase described by a homogeneous composition field, (c_o); an isostructural two-phase mixture with composition differences between the two phases described by an inhomogeneous composition field, c(r); and an ordered single phase with antiphase domain boundaries characterized by an inhomogeneous long-range order parameter field, η(r), and a homogenous composition field (assuming no segregation to antiphase domain boundaries), c_o. In the upper three figures of Figure 1, the microscopic-level morphologies are described by the occupation probabilities of one atomic species on a given lattice site. The field variables c and η are continuous across the interfaces between different phases or between structural domains. Examples of one-dimensional composition profiles before and after an isostructural decomposition are schematically shown in Figure 2. Figure 2a represents a homogeneous single-phase described by a homogeneous composition profile with random small perturbations; Figure 2b shows a two-phase mixture with equilibrium compositions c_α and c_β.

Thermodynamic Driving Force for Microstructural Evolution

As mentioned, the driving force for the temporal evolution of a microstructure is usually a sum of several contributions, including the reduction in the bulk-chemical free energy (F_{bulk}), the interfacial energy (F_{int}), the elastic energy (F_{elast}), and the ener-

gies (F_{appl}) due to applied fields. The total free energy of a system is

$$F_{tot} = F_{bulk} + F_{int} + F_{elast} + F_{appl} \quad (1)$$

While the bulk-chemical free energy depends only on the volume fractions of each constituent phase, all other terms are usually microstructure-dependent. Since the microstructures are described by field variables, in order to model their evolution the free energies have to be formulated as functionals of the field variables; then, the driving forces are defined as the first variational derivatives of the free energies with respect to the field variables. At equilibrium, the total free energy is minimized and the total variational derivative is zero.

Bulk-Chemical Free Energy

In the field approach, the bulk-chemical free energy is described by a local chemical free-energy density function, usually formulated as a Landau-type of polynomial as a function of field variables. At equilibrium, the local free-energy density function is minimized with respect to the field variables. If the initial state is not at equilibrium, there is a bulk driving force for phase transformations, which is best illustrated for the case of simplest isostructural decomposition in which the initial state is a homogeneous single phase; at equilibrium it is a two-phase mixture. The bulk-chemical driving force (per unit volume) for decomposition of the initially homogeneous single phase with composition c_o into an equilibrium two-phase mixture of compositions c_α and c_β is Δf as indicated in Figure 3. The total bulk driving force is the volume integral of Δf.

Interfacial Free Energy

To illustrate how the interfacial energy is introduced into the field model, consider a system that can be described by a single inhomogeneous field, ϕ. The total chemical free energy ($F_{chem} = F_{bulk} + F_{int}$) is then given by[1-3]

$$F_{chem} = \int_v [f(\phi) + k(\nabla\phi)^2]dV \quad (2)$$

where f is the local free-energy density function and k is a positive constant called the gradient-energy coefficient. The gradient term is introduced as an energy penalty on field inhomogeneities such as those that occur at an interface. Therefore, the total excess free energy associated with interfaces, or the total interfacial energy, in the diffuse-interface description is given by the equation

$$F_{int} = \int_v [f(\phi) - f_o(\phi) + k(\nabla\phi)^2]dV \quad (3)$$

where $f_o(\phi)$ is the equilibrium free-energy density of a two-phase mixture, which, for the case of isostructural decomposition, is represented by the common tangent line through c_α and c_β in Figure 3.

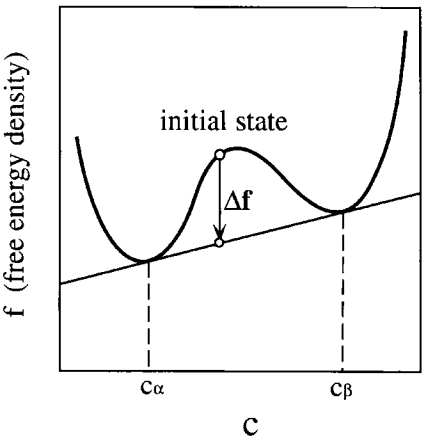

Figure 3. A schematic free-energy density curve as a function of composition showing the driving force for decomposition of a homogeneous solution at composition c_o into a two-phase mixture with equilibrium compositions c_α and c_β is Δf.

Elastic-Strain Energy

To incorporate the elastic-strain energy contribution to the total driving force for microstructural evolution, the strain energy must be formulated as a functional of the field variables. This can be accomplished by expressing the stress-free strain field, $\varepsilon^0_{ij}(r)$, through c(r) if the strain is predominantly caused by the concentration heterogeneity[4] or through $\eta_p(r)$ if the strain is mainly due to the structural-order parameter heterogeneity,[5] for example,

$$\varepsilon^0_{ij}(r) = (c(r) - \bar{c})\varepsilon^{00}_{ij} \quad (4)$$

$$\varepsilon^0_{ij}(r) = \sum_{p=1}^{v} \eta_p^2(r)\varepsilon^{00}_{ij}(p) \quad (5)$$

where $\bar{c}$ is the average composition, v is the number of different orientation variants,

$$\varepsilon^{00}_{ij} = \frac{da}{adc} \quad (6)$$

is a tensor of the concentration expansion coefficient and

$$\varepsilon^{00}_{ij}(p) = \frac{1}{(\eta^0_p)^2}\frac{a_p - a_m}{a_m} \quad (7)$$

where η^0_p is the equilibrium value of the structural order parameter for the product phase and a_p and a_m are the lattice parameters of the equilibrium product and matrix phases at the stress-free state, respectively. The tensors ε^{00}_{ij} and $\varepsilon^{00}_{ij}(p)$ describe the stress-free transformation strains that transform the parent phase into new phase particles in a stress-free state.

By assuming that the parent and product phases have the same elastic constants, close analytical expressions for the strain energy (F_{elast}) as a function of c(r) or $\eta_p(r)$ can be obtained in the Fourier space based on the elasticity theory of Khachaturyan for arbitrary distributions of precipitates.[6] Therefore, all of the information concerning a morphology or microstructure is contained in the field variables c(r) and $\eta_p(r)$, while all of the information on the crystallography of a phase transformation is described by the stress-free strains.

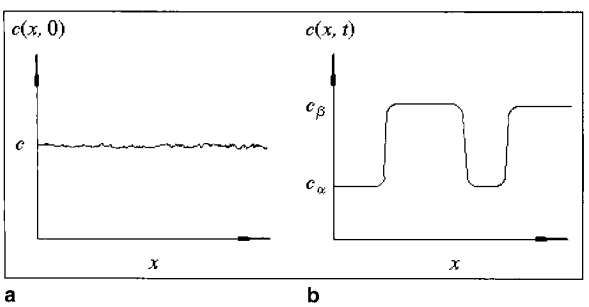

Figure 2. Schematic one-dimensional composition profiles of (a) a homogeneous phase with small random noise and (b) a two-phase mixture of equilibrium compositions c_α and c_β.

Evolution Equations

There are two types of field variables—conserved or nonconserved. The most familiar example of a conserved field variable is the concentration or composition field, which distinguishes the difference in compositions between two phases. An example of a nonconserved field is the long-range order parameter field that describes the local degree of order in ordered alloys with antiphase domains. If ϕ is the conserved concentration field (c), its temporal evolution is governed by a diffusion equation that is, in the diffuse-interface context, usually referred to as the Cahn-Hilliard equation[7]

$$\frac{\partial c}{\partial t} = -\nabla \bullet J \quad (8)$$

where

$$J = -M\nabla(\mu_{chem} + \mu_{elast}) \quad (9)$$

$$\mu_{chem} = \frac{\delta F_{chem}}{\delta c} = f'(c) - k\nabla^2 c \quad (10)$$

$$\mu_{chem} = \frac{\delta F_{elast}}{\delta c} \quad (11)$$

It can be shown that the curvature effect on the chemical potential (i.e., the Gibbs-Thompson effect) is automatically included through the gradient term. In particular, it can be shown that [8]

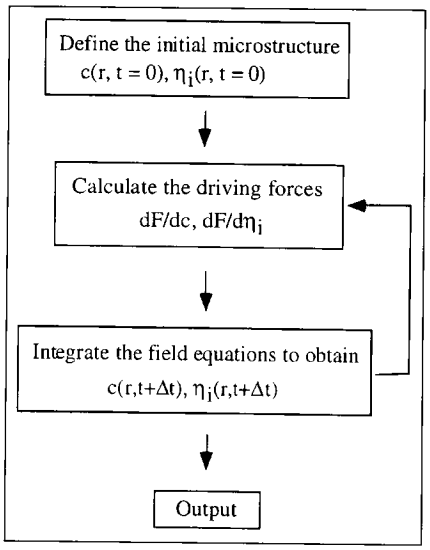

Figure 4. A schematic of the main steps involved in a field simulation.

$$\mu_{chem} = \frac{f_\beta - f_\alpha}{c_\beta - c_\alpha} - \frac{\sigma K}{c_\beta - c_\alpha} = \mu_{chem}^{eq} - \frac{\sigma K}{c_\beta - c_\alpha} \qquad (12)$$

where $c_\beta - c_\alpha$ is the change of concentration across the interface, σ is the interfacial energy per unit area, K is the local mean curvature of an interface, and $f_\beta - f_\alpha$ is the difference between the free energies of the two bulk equilibrium phases.

On the other hand, if a system can be described by a single nonconserved field (e.g., the long-range order parameter field for describing the congruent ordering and antiphase domain coarsening) its evolution is described by a relaxation equation, often called the time-dependent Ginzburg-Landau equation:

$$\frac{\partial \eta(r,t)}{\partial t} = -L\frac{\delta F}{\delta \eta(r,t)} \qquad (13)$$

where L is the relaxation constant.

In general, however, for a given inhomogeneous system, more than one field variable is required to describe a microstructure. The temporal and spatial evolution of field variables are then described by coupled nonlinear diffusion equations for conserved fields c(r,t) and relaxation equations for nonconserved fields. With random thermal noise, both types of equations become stochastic, and their applications to studying critical dynamics have been extensively discussed.[9,10]

Computer Simulation Procedure

In order to carry out a computer simulation of microstructural evolution employing the field approach, four steps must be taken.

- Determine the physically proper field variables for a system under consideration.
- Formulate a local free-energy density function as a function of the chosen field variables that should correctly describe the symmetries and basic thermodynamic behaviors of the system.
- Choose the phenomenological coefficients entering the kinetic equations from experimental measurements or more fundamental calculations.
- Set-up the appropriate initial and/or boundary conditions and numerically solve the field kinetic equations.

Figure 4 illustrates the main steps involved in a computer simulation.

APPLICATIONS

Since the field approach is phenomenological, it can potentially be applied to simulating the microstructural development in a rich variety of material processes by choosing different field variables. Examples of some recent applications are summarized in Table I.

Precipitation of Ordered Intermetallics

Figure 5 shows an example of microstructural evolution during precipitation and coarsening of ordered intermetallic precipitates in an initially metastable disordered solid solution, obtained from a two-dimensional computer simulation with 256 × 256 grid points.[25] Two fields—a concentration field and a long-range order parameter field—were introduced. The local free-energy density, f(c, η), was assumed to be a polynomial with second-order in c and six-order in η

$$f(c,\eta) = \frac{1}{2}A(c-c')^2 + \frac{1}{2}B(c''-c)\eta^2 - \frac{1}{4}C\eta^4 + \frac{1}{6}D\eta^6 \qquad (14)$$

where A, B, C, D, c′, and c″ are phenomenological constants. The free energy of the disordered phase can be obtained by setting the value of the long-range order parameter equal to zero [i.e., f(c,η = 0)]. The free energy of the ordered phase can be calculated by replacing η by using the equilibrium long-range order parameter as a function of composition, η_0(c) [i.e., f(c, η_0(c)]. Their common tangent determines the equilibrium compositions of the two coexisting phases as shown in Figure 6 for a specific set of constants, A = 7.5, B = 4.0, C = 1.0, D = 0.5 (measured in an energy unit equal to the typical chemical driving force |Δf|), c′ = 0.1, and c″ = 0.5. The gradient-energy coefficients were chosen in such a way that the interphase and antiphase domain boundary energies are isotropic. The elastic modulus is assumed to be homogeneous with a negative cubic elastic anisotropy; the elastic strain is assumed to be mainly due to the compositional inhomogeneities. In addition, the stress-free strain is assumed to be purely dilatational. Nucleation of the ordered precipitate particles was simulated by thermal fluctuations introduced through the noise terms added to the right sides of the kinetic equations.

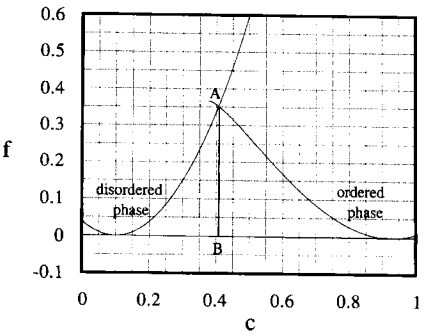

Figure 5. A two-dimensional projection of the local free-energy minima with respect to long-range order parameter on the f-c plane. $\overline{AB}$ designates the typical driving force Δf.

The microstructures were visualized by gray levels representing different values of the local composition, c(r,t), except for Figure 6a, where the values of η(r,t) were represented. At the initial stage, two kinds of ordered domains, represented by black and white for $\eta > 0$ and $\eta < 0$, nucleate as near-circular particles with a near-random distribution (Figure 6a). As the particles grow in size, they gradually transform into square-like shapes, and spatial correlation be-

Table I. Examples of the Field Model Applications

Types of Processes	Field Variables	References
Isostructural Spinodal Decomposition	c	4, 9, 11, 12
Ordering and Antiphase Domain Coarsening	η	13, 14
Solidification in Single-Component Systems	η	15–19
180° Ferroelectric Domain Formation	P (polarization)	20
Solidification in Alloys	c, η	21–24
Precipitation of Ordered Intermetallics with		
Two Kinds of Ordered Domains	c, η	25–27
Four Kinds of Ordered Domains	c, η_1, η_2, η_3	27, 28
90° Ferroelectric Domain Formation	P_1, P_2, P_3	29, 30
Cubic→Tetragonal Displacive Transformation or Martensitic Transformation	η_1, η_2, η_3	31, 32
Tetragonal Precipitates in a Cubic Matrix	c, η_1, η_2, η_3	33, 34
Ordered Precipitate Morphology under Stress	c, η_1, η_2, η_3	35
Grain Growth in a Single-Phase Material	η_1, η_2,..., η_Q	36
Grain Growth in a Two-Phase Mixture	c, η_1, η_2,..., η_Q	37

tween particles (alignment along the elastically soft <10> directions) starts to develop. It may be pointed out that both the shape transition and spatial correlation are entirely caused by the morphology-dependent anisotropic elastic interactions since the interfacial energies are isotropic. Subsequent coarsening of the precipitates takes place via two different mechanisms—coalescence between neighboring particles and normal Ostwald ripening. Finally, a rafting structure consisting of chains of alternating square- or rectangular-shaped precipitate particles is formed (Figure 6d). Although the simulation was performed in two dimensions, the predicted microstructures show remarkable qualitative agreement with experimental observations[38] (Figure 7).

Martensitic Transformations

A second example is shown in Figure 8 for the case of a martensitic transformation, obtained from a three-dimensional simulation.[32] A cubic → tetragonal transformation in an elastically isotropic model system was considered, which results in three orientation variants of the tetragonal phase with the tetragonal axes along [100], [010], or [001] directions of the cubic phase. Therefore, three nonconserved order parameter field—η_1, η_2, and η_3—are introduced to describe the three orientation variants (Figure 9). The local free-energy density function is approximated by a six-order polynomial with respect to the three structural order parameters, which characterizes a first-order transition. It has a local minimum at $\eta = 0$ and six degenerated global minima at $\eta = \pm\eta_1^0, \pm\eta_2^0, \pm\eta_3^0$. Interfacial energies are assumed to be isotropic.

The simulation was started from a homogeneous cubic solid solution described by $\eta_1(r) = \eta_2(r) = \eta_3(r) = 0$, which is metastable with respect to the formation of the tetragonal orientation domains. The nucleation process was modeled by the Langevin noise terms added into the kinetic equations.

Since the field approach does not impose any constraint on the transformation path, it allows the system itself to choose the optimal evolution path and to adopt the optimal structural configurations corresponding to a critical nucleus. To determine the critical nucleus configuration, the noise terms were artificially turned off after a certain period of time in the simulation. Under this condition, all heterogeneities corresponding to the noncritical fluctuations will eventually disappear and the surviving heterogeneities are the critical or operational nuclei.

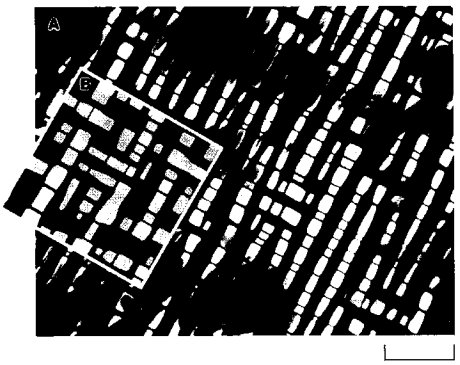

Figure 7. A comparison between experimental observation and simulation prediction of the discontinuous rafting structure in nickel-based superalloys showing (a) a transmission electron microscopy micrograph of Ni-Al-Mo aged 2,330 hours at 775°C (courtesy of M. Fährmann) and (b) the simulation prediction shown in Figure 6d.

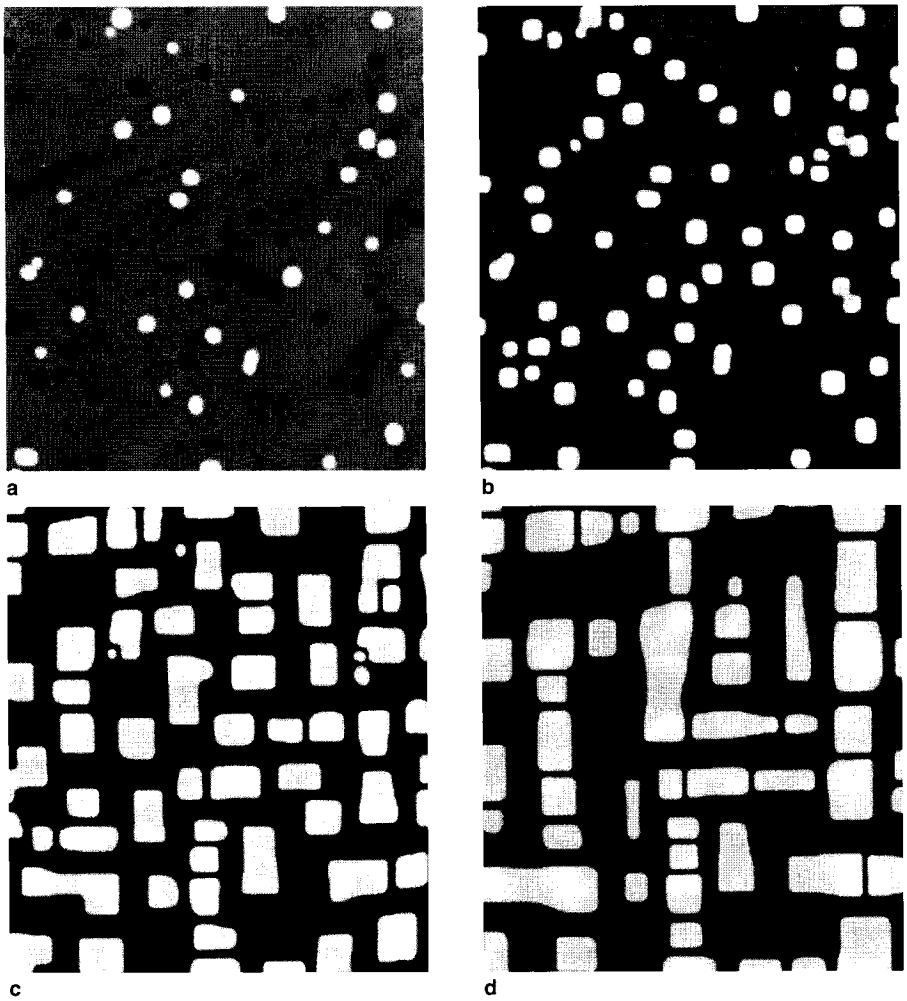

Figure 6. The microstructural evolution during precipitation of an ordered intermetallic phase from a disordered matrix when (a) $\tau = 10$; (b) $\tau = 20$; (c) $\tau = 300$; (d) $\tau = 5{,}000$, where τ is measured in a reduced time unit, $\tau = \tau M|\Delta f|$, M is defined in Equation 9, and Δf is the typical driving force. The white and black particles in (a) are in antiphase relation to each other.

Figure 8a shows the morphology of a survived nucleus after switching off the noise terms. For the sake of simplicity, only two of the three orientation variants—η_1 and η_2—were considered in this simulation. The nine small squares in each micrograph are the consecutive two-dimensional cross sections of a three-dimensional cube with $64 \times 64 \times 64$ mesh points. The sections are perpendicular to the [010] axis of the cubic phase and are equally spaced. The gray level describes $|\eta_1(r)| - |\eta_2(r)|$, with high values represented by white. Therefore, the white and black regions represent two different orientation variants of the tetragonal martensitic phase and the gray background represents the cubic matrix. It can be seen in Figure 8a that all the nuclei are polydomains consisting of twin-related two-orientation variants. This transformation path is drastically different from that usually assumed by the classical nucleation theory in which nucleation is considered as a single particle event. This simulation result demonstrates that the homogeneous nucleation in a martensitic transformation is most likely a multiparticle event with the nucleus consisting of several orientation domains arranged into a spatially correlated group (polytwin structure) to accommodate the elastic strain.

Figures 8b through 8d show how these polydomain nuclei evolve into martensitic plates during subsequent growth and coarsening. Two intersecting martensitic plates with different habit planes—(110) and (101)—are formed at

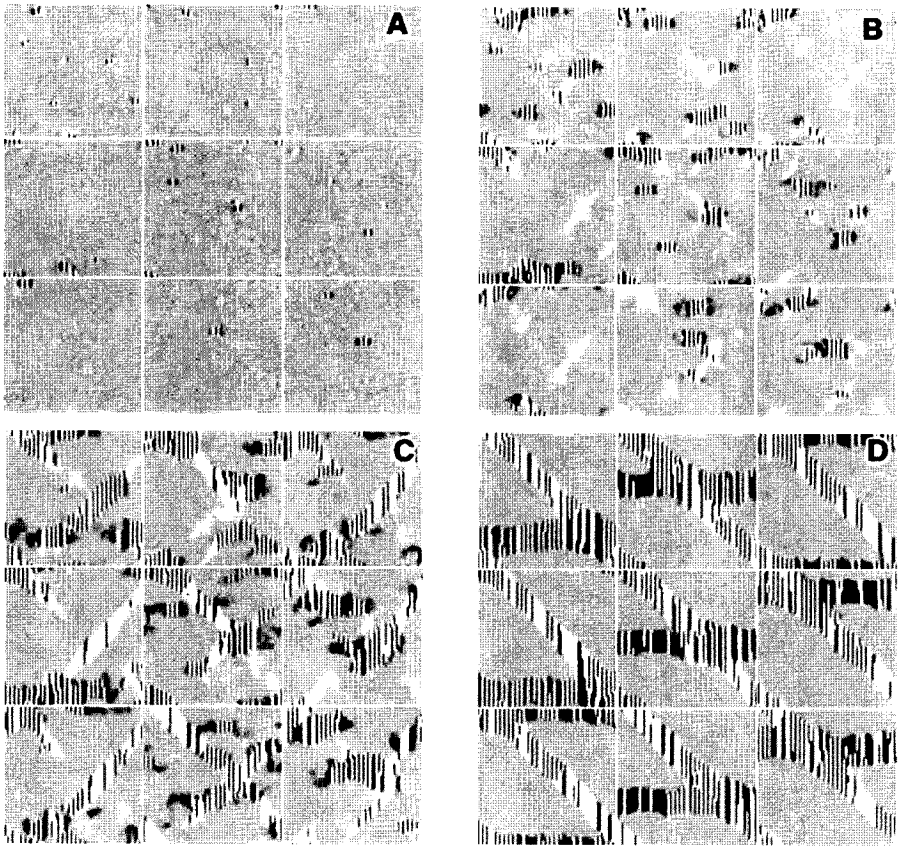

Figure 8. The microstructure development during martensitic transformation through homogeneous nucleation when (a) $\tau = 2$, (b) $\tau = 6$, (c) $\tau = 10$, and (d) $\tau = 20$, where $\tau = tL|\Delta f|$. The nine small squares in each micrograph are the consecutive two-dimensional cross sections of a three-dimensional cube along the [010] axis.

late stages. They are at equilibrium with the cubic parent phase matrix. Extending the aging time did not change the volume fraction of the martensite. The habit planes are determined by the ratio of the volume fractions of the two-orientation variants composing the plates, and they coincide with the habit planes predicted from the invariant plane strain condition.

Grain Growth

The final example is an application of the field model to grain growth in a single-phase system, in which grains of a given crystallographic orientation are represented by a large set of nonconserved order parameter fields.[36] An example of microstructural evolution obtained from a two-dimensional simulation with 512×512 grid points is shown in Figure 10, in which 36 nonconserved field variables were introduced. The local free energy f is chosen such that it has p degenerate minima with equal depth located at $(\eta_1,\eta_2,...\eta_{36}) = (1,0,...,0), (0,1,...,0), ..., (0,0,...,1)$. The grain-boundary energies were assumed to be isotropic. The initial condition was specified by assigning small random values to all field variables at every grid point (e.g., $-0.001 < \eta_i < 0.001$), simulating a liquid. The microstructure was represented by defining the field variables

$$\varphi(r) = \sum_{i=1}^{p} \eta_i^2(r) \qquad (15)$$

which were displayed by gray levels with low and high values represented by dark and bright colors, respectively. Since the values within the domains are high while those at the boundaries are low, the bright regions are grains and the dark lines are grain boundaries. Since the initial values for η_i are essentially zero, the very early stage of the simulation corresponds to crystallization (i.e., the growth of η_i values at different locations driven by the bulk free-energy change). A well-defined grain structure was formed after a short time, and all the bulk driving force was consumed very rapidly. Further microstructural evolution was driven by the excess free energies associated with the grain boundaries, resulting in growth of overall microstructure scales or grain size.

With the temporal microstructural evolution, all the statistical information about the microstructure such as the average grain size, size distribution, average number of sides, side distribution, and local topological changes can be obtained.[39] In addition to grain growth in single-phase materials, the continuum-field method has also been applied to modeling the coupled grain growth and Ostwald ripening in two-phase solids[37] and coarsening of a solid-liquid mixture at high volume fractions of solids.[40]

DISCUSSION

One of the main advantages of the field approach is that any arbitrary microstructure can be easily treated since the interfaces are not singular surfaces requiring imposition of special boundary conditions, but are just regions where the fields have very high gradients. In addition, different thermodynamic driving forces for microstructural evolution, including bulk-chemical free energy, interfacial energy, elastic-strain energy, magnetic energy, electrostatic energy, and applied fields, and, hence, different processes such as nucleation, growth, coarsening, and field-induced domain switching can be described within the same physical and mathematical model. Finally, in the diffuse-interface field model, it is straightforward to take into account long-range diffusion, which takes place, for example, during precipitation of second-phase particles, solute segregation, and second-phase precipitation at grain boundaries in a polycrystalline material.

It should be pointed out that, similar to the conventional sharp-interface approach, the field model gives no direct information on the atomic structure of different equilibrium and nonequilibrium phases and interfacial boundaries. Computationally, simulations using the

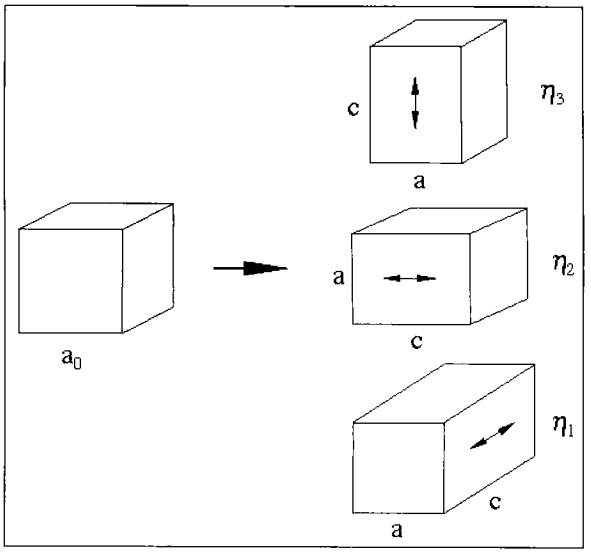

Figure 9. Cubic → tetragonal transformation producing three orientation variants represented by three nonconserved order parameters.

field model are still quite intensive. For example, a typical grain-growth simulation with 512×512 uniform grid points and 36 orientation variables using the simple, forward Euler technique for numerical integration takes about five hours of computer processor unit (CPU) time on a Cray-C90 supercomputer, and for a typical simulation of Martensitic transformation using $64 \times 64 \times 64$ uniform grid points, it requires about two hours of CPU time and 48 megabytes of memory. Therefore, new fast algorithms and techniques for solving the kinetic equations will be very beneficial for the practical applications of the field model to large-scale simulations.

Finally, as demonstrated in the example of precipitation of ordered intermetallic precipitates and others, excellent agreements between predicted and experimentally observed microstructures can be achieved, at least qualitatively, using the field model (e.g., in terms of the sequence of phase transformations, shape evolution, and mutual arrangement of precipitate particles) as long as the model incorporates the essential physics involved in a given process. Even some quantitative information such as the growth exponent of the average particle size as a function of time and particle size distributions in the scaling regime seems to be rather insensitive to the specific parameters employed in the simulation. However, if quantitative information on the absolute coarsening rate of a microstructure is desired, the effect of the accuracy of the time and spatial discretization of the kinetic field equations might be significant and must be considered.

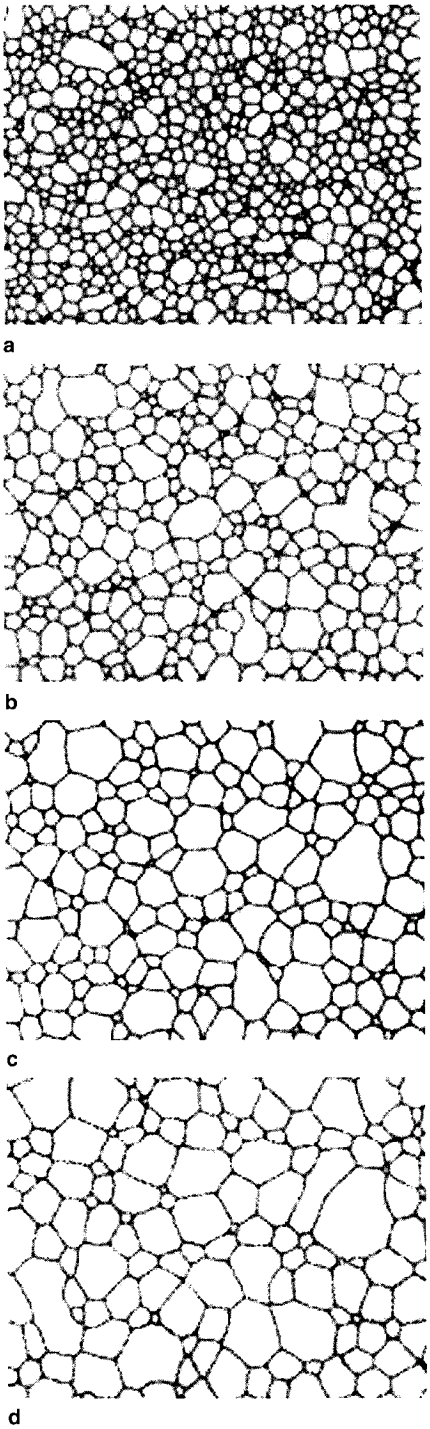

Figure 10. The microstructural evolution during grain growth using 36 nonconserved field variables and a two-dimensional simulation with a 512×512 grid points. t = the number of time steps in the simulation. (a) t = 1,000, (b) t = 3,000, (c) t = 5,000, and (d) t = 8,000.

ACKNOWLEDGEMENT

The authors acknowledge the financial support of the U.S. National Science Foundation, the Ohio State University, the U.S. Office of Naval Research, and the Advanced Research Projects Agency/National Institute of Standards and Technology program on mathematical modeling of microstructures in advanced alloys. The simulations were performed at the Pittsburgh Supercomputing Center.

References

1. J.S. Rowlinson, translation of a 1893 paper by J.D. van der Waals, "Thermodynamic Theory of Capillarity under the Hypothesis of a Continuous Variation of Density," *J. Statistical Physics*, 20 (1979), p. 197.
2. L.D. Landau, *JEPT*, 7 (1937), p. 19; L.D. Landau, *JEPT*, 7 (1937), p. 627; E. M. Lifshitz, *JEPT*, 11 (1941), p. 269; E. M. Lifshitz, *JEPT*, 14 (1944), p. 353.
3. J.W. Cahn and J.E. Hilliard, *J. Chem. Phys.*, 28 (1958), p. 258.
4. Y. Wang, L.-Q. Chen, and A.G. Khachaturyan, *Acta Metall. Mater.*, 41 (1993), p. 279; *Phys. Rev. B*, 46 (1992), p. 11194.
5. L Q. Chen, Y. Wang, and A.G. Khachaturyan, *Phil. Mag. Lett.*, 65 (1992), p. 15.
6. A.G. Khachaturyan, *Soviet Phys. Solid St.*, 9 (1968), p. 2040; A.G. Khachaturyan, *Theory of Structural Transformations in Solids* (New York: Wiley, 1983).
7. J.W. Cahn, *Acta Metall.*, 9 (1961), p. 795; J.W. Cahn, *Acta Metall.*, 10 (1962), p. 179.
8. A.J. Bray, *Adv. in Phys.*, 43 (1994), p. 357.
9. P.C. Hohenberg and B.I. Halperin, *Rev. Mod. Phys.*, 49 (1977), p. 435.
10. J.D. Gunton, M.S. Miguel, and P.S. Sahni, *Phase Transitions and Critical Phenomena*, vol. 8. ed. C. Domb and J.L. Lebowitz (New York: Academic Press, 1983), pp. 267–466.
11. T.M. Rogers, K.R. Elder, and R.C. Desai, *Phys. Rev. B*, 37 (1988), p. 9638.
12. A. Onuki, *J. Phy. Soc. Jpn.*, 58 (1989), p. 3065; *J. FY. Soc. Jpn.*, 58 (1989), p. 3069; H. Nishimori and A. Onuki, *Phys. Rev. B*, 42 (1990), p. 980.
13. S.M. Allen and J.W. Cahn, *Acta Metall.*, 27 (1979), p. 1085.
14. Y. Oono and S. Puri, *Phys. Rev. Lett.*, 58 (1987), p. 836.
15. J.S. Langer, *Condensed Matter Physics*, ed. G. Grinstein and G. Mazenko (Singapore: World Scientific, (1986), p. 165.
16. R. Kobayashi, *Experim. Math.*, 3 (1994), pp. 59–81.
17. A. A. Wheeler, W.J. Boettinger, and G.B. McFadden, *Phys. Rev. A*, 45 (1992), pp. 7424–7439.
18. G. Caginalp and E. Socolovsky, *J. Sci. Comput.*, 15 (1994), pp. 106–126.
19. A. Karma and W.-J. Rappel, *Mathematics of Microstructures*, ed. L.Q. Chen et al. (Joint SIAM-TMS proceedings, to be published).
20. W. Yang and L.-Q. Chen, *J. Am. Ceram. Soc.*, 78 (1995), p. 2554.
21. A. A. Wheeler, W.J. Boettinger, and G.B. McFadden, *Phys. Rev. A*, 47 (1993), p. 1893.
22. J.A. Warren and W.J. Boettinger, *Acta Metall. Mater.*, 43 (1995), p. 689.
23. K.R. Elder et al., *Phys. Rev. Lett.*, 72 (1994), p. 677.
24. Alain Karma, *Phys. Rev.*, E49 (1994), p. 2245.
25. Y. Wang and A.G. Khachaturyan, *Scripta Metall. et Mater.*, 31 (1995), p. 1425; Y. Wang, Ph.D. thesis, Department of Ceramics, Rutgers University (1995); Y. Wang and A.G. Khachaturyan, *Phil. Mag. A*, 72 (1995), p. 1161.
26. Y. Wang, L.Q. Chen, and A.G. Khachaturyan, *Solid→Solid Phase Transformations*, ed. W.C. Johnson et al. (Warrendale, PA: TMS, 1994), pp. 245–265.
27. T. Eguchi, K. Oki, and S. Matsumura, *MRS Symp. Proc.*, vol. 21 (1984), p. 589; K. Shiiyama et al., *Proceedings of the International Workshop on Computational Materials Science* (IWCMS) (1990), pp. 103–110.
28. Y. Wang and A.G. Khachaturyan, to be published.
29. S. Nambu and D.A. Sagala, *Phys. Rev.*, B 50 (1994), p. 5838.
30. H.L. Hu and L.Q. Chen, unpublished.
31. D.N. Fan and L.Q. Chen, *J. Am. Ceram. Soc.*, 78 (1995), p. 769.
32. Y. Wang and A.G. Khachaturyan, accepted in *Acta Mater.* (1996).
33. Y. Wang et al., *J. Am. Ceram. Soc.*, 76 (1993), p. 3029; Y. Wang et al., *J. Am. Ceram. Soc.*, 78 (1995), p. 657.
34. D.N. Fan and L.Q. Chen, *J. Am. Ceram. Soc.*, 78 (1995), p. 1680.
35. D.Y. Li and L.Q. Chen, accepted in *Acta Mater.* (1996); unpublished (1996).
36. L.Q. Chen and W. Yang, *Phys. Rev.*, B50 (1994), p. 15752; L.Q. Chen, *Scripta Metall. et Mater.*, 32 (1995), p. 115; D.N. Fan and L.Q. Chen, accepted in *Acta Mater.* (1996).
37. L.Q. Chen and D.N. Fan, *J. of the Am. Ceram. Soc.*, 79 (1996), p. 1163; D.N. Fan and L.Q. Chen, accepted in *Acta Mater.* (1996); D.N. Fan and L.Q. Chen, submitted to *J. Am. Ceram. Soc.* (1996).
38. M. Fährmann, unpublished work.
39. D.N. Fan, and L.Q. Chen, accepted in *Acta Mater.* (1996).
40. D.N. Fan, Ph.D. thesis, Department of Materials Science and Engineering, Pennsylvania State University (1996).

ABOUT THE AUTHORS

Long-Qing Chen earned his Ph.D. in materials science and engineering at Massachusetts Institute of Technology in 1990. He is currently an assistant professor of materials science and engineering at Pennsylvania State University.

Yunzhi Wang earned his Ph.D. in materials science and engineering at Rutgers University in 1995. He is currently an assistant professor of materials science and engineering at Ohio State University.

For more information, contact L.-Q. Chen, Pennsylvania State University, 118 Steidle Building, University Park, Pennsylvania 16802; (814) 863-8101; fax (814) 865-0016; e-mail chen@ems.psu.edu.